# Conformation of Poly(ethylene oxide) Intercalated in Clay and $MoS_2$ Studied by Two-Dimensional Double-Quantum NMR

**D. J. Harris,[†] T. J. Bonagamba,[*,†,‡,§] and K. Schmidt-Rohr[*,†,||]**

*Polymer Science and Engineering Department, University of Massachusetts, Amherst, Massachusetts 01003, and Instituto de Física de São Carlos, Universidade de São Paulo, PO Box 369, São Carlos, São Paulo, Brazil 13560-970*

*Received May 18, 1999; Revised Manuscript Received August 2, 1999*

ABSTRACT: The conformation of poly(ethylene oxide), PEO, intercalated in layered clays and $MoS_2$ has been characterized by double-quantum solid-state NMR. Using PEO with 13% $^{13}C-^{13}C$ labeled units, the conformational statistics of the OC−CO bonds have been determined. The OC−CO bonds of the polymer in narrow interlayer gaps of ∼0.8, ∼0.85, and ∼1.0 nm thickness consistently exhibit a high gauche content of approximately 90%. This rules out models with highly trans-containing chains as found in certain complexes of PEO with $HgCl_2$ or *p*-nitrophenol.

## Introduction

The intercalation of organic compounds in layered inorganic solids such as smectite clay minerals (montmorillonite and hectorite) and transition metal dichalcogenides ($MoS_2$ and $TiS_2$) has been widely studied during the last few years.[1−16] Recently, the interest in the nanocomposites of poly(ethylene oxide), PEO, $[(-CH_2-CH_2-O-)_n]$, increased due to their unique electronic, ionic (without counterions), mixed electronic and ionic, structural, and mechanical properties.[6,9] The knowledge of the conformational characteristics of PEO in these nanocomposites is therefore a prerequisite to understanding the above-cited important properties. Nevertheless, the structure of PEO in the less than 1 nm wide gaps between the inorganic layers is not well characterized. In this paper, the conformation of PEO intercalated in smectite clays and a transition metal dichalcogenide is determined by two-dimensional double quantum solid-state nuclear magnetic resonance (NMR) spectroscopy.

It was found 3 decades ago[17,18] by wide-angle X-ray diffraction (WAXD), infrared (IR), and Raman spectroscopic methods that a PEO chain in the crystalline state has a helical structure which contains seven units and turns twice in the fiber identity period of 1.93 nm; see Figure 1b. In this helix, the OC−CO torsions are gauche, ranging from 49 to 92° in the proposed crystal structure,[19] while the CO−CC torsions are in the trans conformation. The cross section area of the PEO $7_2$ helix is approximately $\pi/4$ (0.52 nm)$^2$. The PEO conformation in the intercalates may differ from the $7_2$ helical structure. WAXD measurements[1,5,8] show that the formation of PEO intercalates involves a gallery expansion by 0.4 or 0.8 nm, depending on the polymer mass fraction used to prepare the intercalated material; see Figures 1 and 2. The estimated heights of the galleries, including the alkali ions, in a smectite clay (hectorite) and in a transition metal dichalcogenide ($MoS_2$) are 0.80−1.00 and 0.85 nm, respectively; see Table 1.

**Table 1. Composition and Interlayer Distances of the Samples Studied**

| sample[a] | *R* | host *c* (nm) | nanocomposite *c* (nm) | Δ*c* (nm) | $gap_0$ (nm)[b] | $gap_1$ (nm)[b] |
|---|---|---|---|---|---|---|
| (1) PEO/MMT(0.40) | 0.10 | 0.97 | 1.37 | 0.40 | 0.35 | 0.75 |
| (2) PEO/MMT(0.80) | 0.40 | 0.97 | 1.77 | 0.80 | 0.35 | 1.15 |
| (3) PEO/HCT(0.45) | 0.10 | 0.98 | 1.43 | 0.45 | 0.35 | 0.8 |
| (4) PEO/HCT(0.70) | 0.40 | 0.98 | 1.68 | 0.70 | 0.35 | 1.0 |
| (5) PEO/$MoS_2$(0.82) | 0.45 | 0.61 | 1.43 | 0.82 | 0.02 | 0.85 |

[a] The number in parentheses is the parameter Δ*c* in nm. [b] Estimated interlayer gap before, $gap_0$, and after intercalation, $gap_1$.

In the nanocomposites, the polymer conformation may be affected by the limited space between layers and by the polymer interaction with the charged surfaces of the inorganic host layers and interlayer cations,[1,4] such as $Li^+$ or $Na^+$. Three particular models have been proposed: (1) preservation of the PEO helical conformation for the 0.8 nm compounds[5]; (2) double-polymer-layer planar zigzag disposition for the 0.8 nm compounds;[5] (3) adsorption of the polymer layer on the inorganic host surfaces for both 0.4 or 0.8 nm compounds, resulting in single or double polymer layers, respectively[1].

Various thermal studies[1−5,7−10] show no evidence of a crystalline melting transition or a glass transition in the nanocomposites, which indicates that the confinement of the polymer chain between the inorganic layers prohibits bulklike crystallization. This also suggests that the polymer conformation within the galleries may be different than that of neat PEO. Adsorption isotherms show only one plateau,[5] indicating that the chains do not form double layers in these nanocomposites.

In this work, the conformations of the OC−CO bonds of PEO intercalated in hectorite and in $MoS_2$ are investigated using double-quantum solid-state $^{13}C$ NMR (DQ−NMR).[20] DQ−NMR yields two-dimensional (2D) spectra in which the first dimension shows the sum of the orientation dependent $^{13}C$ chemical shifts, while the second dimension shows the individual anisotropic chemical shifts and $^{13}C-^{13}C$ dipolar coupling. These 2D

* To whom correspondence should be addressed.
[†] University of Massachusetts.
[‡] Universidade de São Paulo.
[§] Telephone: (413) 577-1436. Fax: (413) 545-0082. E-mail: tito@polysci.umass.edu.
[||] Telephone: (413) 577−1417. Fax: (413) 545−0082. E-mail: srohr@polysci.umass.edu.

10.1021/ma9907800 CCC: $18.00 
Published on Web 09/08/1999

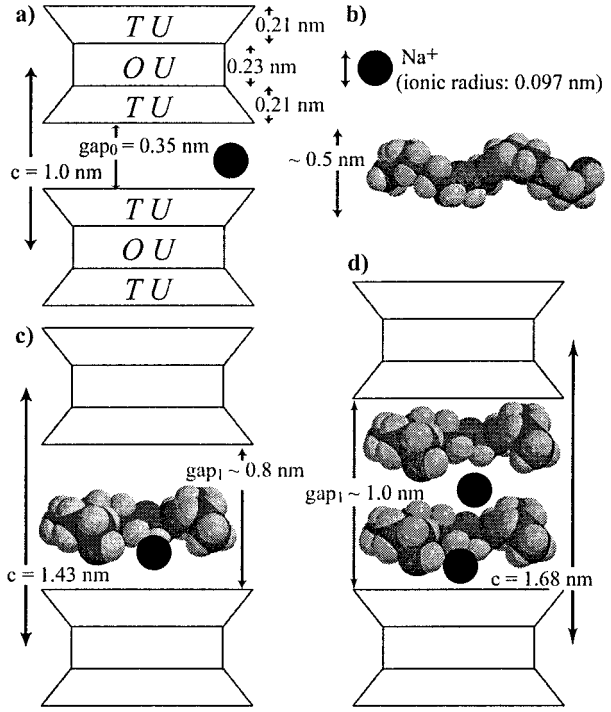


**Figure 1.** Idealized structures of smectite clays (montmorillonite and hectorite), PEO, and the respective intercalated nanocomposites. Smectite silicate clay minerals have layer lattice structures in which oxyanions are separated by layers of hydrated cations.[33] (a) The oxygen atoms define the upper and lower sheets of tetrahedral units (TU) and the central sheet of octahedral units (OU). Si and sometimes Al normally occupy the tetrahedral positions in the oxygen framework. Al, Mg, or Li may occupy octahedral sites. In montmorillonite, the layer charge originates from the substitution of octahedral $Al^{3+}$ by $Mg^{2+}$, while in hectorite from the substitution of octahedral $Mg^{2+}$ by $Li^{+}$. The naturally occurring clays contain other ions by isomorphous substitution such as iron. Typically, the charge deficiency in the layers of smectites ranges from 0.4 to 1.2 electrons per $Si_8O_{20}$, which is balanced by interlayer ions ($Na^{+}$ in MMT and HCT). (b) Crystalline PEO conformation proposed by Tadokoro is shown.[19] (c and d) Idealized structures for the intercalated nanocomposites PEO/HCT(0.45) (c) and PEO/HCT(0.70) (d) are shown, taking into consideration the information obtained from our WAXD and double-quantum NMR measurements. The main purpose is the representation of the relevant length scales; many details of the polymer conformation and cation distribution are hypothetical.

spectra depend on the relative orientations of the coupled sites and thus on the OC−CO torsion angles. By matching the experimental 2D spectrum with simulated 2D patterns, one can quantify the fraction of trans and gauche OC−CO torsion angles. In the PEO used for these studies, 13% of the repeat units are $^{13}C-^{13}C$ labeled.

## Experimental Section

**Materials. Synthesis of (−$^{13}$C−$^{13}$C−O−) PEO.** $^{13}C-^{13}C$ labeled PEO was synthesized by anionic polymerization in THF using K−naphthalene as the initiator. Approximately 3.5 g of unlabeled ethylene oxide gas (Aldrich) and 0.5 g of ethylene-$^{13}C_2$ oxide gas (Cambridge Isotope Laboratories) was dried with calcium hydride and then polymerized at room temperature for 72 h. The yield after precipitation in hexanes was 90%. Gel permeation chromatography with a light-scattering detector and using $CH_2Cl_2$ as the eluent determined $M_n$ to be 27 000 and $M_w$ to be 30 000. The polydispersity index was calculated to be 1.10. $^1$H NMR determined that 13% of the ethylene oxide units are doubly labeled.

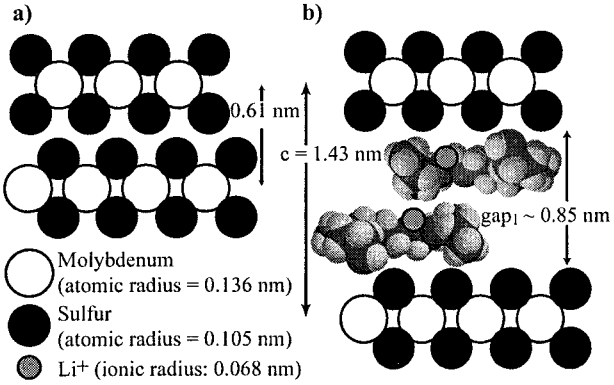


**Figure 2.** Idealized structures of $MoS_2$ and the respective PEO intercalated nanocomposites. (a) In the $MoS_2$ layer structure, the molybdenum is sandwiched between two sulfur sheets with six atoms of S surrounding a Mo atom, forming a trigonal prism. These layers are stacked along the *c* axis, with a long period $c = 0.615$ nm. (b) Idealized structure of the intercalated nanocomposite PEO/$MoS_2$(0.82) is shown, based on our WAXD and double-quantum NMR measurements.

**PEO Intercalation in Clays.** The $Na^{+}$−hectorite (SHCa-1) and $Na^{+}$−montmorillonite (SWy-1), both from the Source Clay Minerals Repository, University of Missouri−Columbia, were prepared for the intercalation process using procedures similar to those described elsewhere.[1,5] $Na^{+}$−hectorite (HCT) was first treated with 0.5 N acetic acid in order to eliminate carbonate impurities. Afterward, the clay was dissolved in deionized water and filtered several times.[5] $Na^{+}$−montmorillonite (MMT), which was used as an important reference material, was dissolved in deionized water and filtered several times in order to remove noncolloidal impurities such as quartz and feldspar.[1] No ion exchange was performed. After this purification process, the $Na^{+}$−clays were dried in an oven at 65 °C and then were heated to 80 °C under vacuum for several days. These dried $Na^{+}$−clays, sealed in capillary tubes, were analyzed by WAXD in order to determine the interlayer gap.

Nanocomposites were obtained by the stoichiometric addition of PEO and $Na^{+}$−clays in acetonitrile. Two reaction stoichiometries were used for the preparation of layered nanocomposites:[1] $R = 0.1$ and 0.4 ($R$ = g of PEO/g of clay), to obtain uniform gallery expansions of 0.4 and 0.8 nm, respectively. These reactions involved 300 or 150 mg of clay and 30 or 60 mg of PEO dissolved in 20 mL of acetonitrile. The colloidal suspension was stirred for ca. 24 h at room temperature and filtered, and then the nanocomposite was dried following the procedure described above. These $Na^{+}$−clay nanocomposites were immediately sealed in appropriate glass tubes for NMR and WAXD and in aluminum pans for DSC. For the stoichiometry of $R = 0.4$, excess PEO was eliminated by repeatedly washing with deionized water,[5] and the DSC did not show a melting peak.

Like most naturally occurring silicates, montmorillonite contains some $Fe^{3+}$ substitutionally situated in lattice $Al^{3+}$ sites. The presence of this paramagnetic impurity induces strong line broadening in $^{13}$C NMR.[21] For this reason, the intercalated PEO−montmorillonite nanocomposites could not be studied by $^{13}$C NMR. However, given that montmorillonite is one of the most widely studied clay materials while hectorite is less commonly used, the scattering curves for montmorilonite are included below as references for those of the hectorite samples that were used for NMR spectroscopy due to their lower abundance of paramagnetic elements.[5]

**PEO Intercalation in $MoS_2$.** $MoS_2$ (Aldrich) was dried and then immediately analyzed by WAXD in order to determine the width of the gap between layers. The $MoS_2$ nanocomposites were obtained by reduction to $LiMoS_2$ and reaction with aqueous PEO.[2,6,22] To prepare the $Li_xMoS_2$ ($x \approx 1$) the host (0.5 g) was reduced with about a 35% molar excess of *n*-butyllithium (1.67 mL, 2.5 M in hexane) in a solution of 100 mL of dry and $O_2$-free hexane.[23] This solution was stirred for about

1 day under nitrogen atmosphere. The solution was filtered, and the $LiMoS_2$ was then immersed in deionized and $O_2$-free water (60 mL) containing a stoichiometric amount of PEO and stirred for ca. 30 h.[2,6,23] Since there is no evidence of intercalation producing 0.4 nm gallery expansion, only one reaction stoichiometry was used for the preparation[2] of layered nanocomposites derived from $MoS_2$: $R = 0.45$. The solid product was separated by centrifugation at 12 000 rpm and washed several times with deionized and $O_2$-free water to ensure removal of LiOH and other soluble impurities.[2] During the intercalation of PEO in $MoS_2$, all manipulations were performed under an $N_2$ atmosphere to exclude oxygen.[2] The products were carefully dried under vacuum at a temperature of ca. 80 °C for several days. After that, the fine powdered samples were sealed in appropriate glass tubes for NMR and WAXD and aluminum pans for DSC.

Table 1 summarizes the characteristics of all samples prepared, including the abbreviation for each intercalate.

**Methods. Sample Characterization.** Elemental analyses were performed using two instruments. Carbon and hydrogen quantification was done using a 240XA elemental analyzer employing a modified Pregl-Dumas technique, while lithium concentration was measured utilizing a Perkin-Elmer 403 AA spectrometer in the emission mode.

**Wide-Angle X-ray Diffraction.** WAXD studies were performed using a Siemens D500 instrument with a Ni-filtered Cu Kα radiation source in transmission mode.

**Differential Scanning Calorimetry (DSC).** DSC measurements were performed with 10-mg samples loaded in Al pans on a DuPont Instruments DSC 2910 equipment. Samples were heated at 10 °C/min from −90 to +100 °C.

**NMR Experiments.** The two-dimensional double-quantum NMR spectra were recorded on a Bruker MSL 300 spectrometer at a $^{13}C$ resonance frequency of 75.5 MHz in a 5-mm diameter coil of a static variable temperature probe. The $^{13}C$ and $^{1}H$ 90° pulse lengths were ca. 3.5 $\mu$s. A cross-polarization time of 500 $\mu$s and a signal-acquisition time of 2.8 ms were used. For the PEO/HCT intercalated nanocomposites, the recycle delay was 0.5 s ($T_1$ is short) due to the presence of paramagnetic impurities and the spectra were obtained at 225 K, while for the PEO/$MoS_2$ it was 1 s and $T = 220$ K. These low temperatures were necessary to avoid motion of the PEO chains during the double-quantum excitation and reconversion delays. In the $t_1$ dimension, 30 slices with increments of 28 $\mu$s were acquired. Only one value of double-quantum excitation and reconversion delay was utilized, $2\tau = 280$ $\mu$s. The measuring time for each two-dimensional double-quantum spectrum was ca. 24 h. To improve the signal-to-noise ratio of the spectra, two acquisitions of 24 h were added.

The simulated 2D spectra were calculated directly in the frequency domain, by scanning the $\mathbf{B_0}$ direction over all directions.[20,24,25] For each orientation and specified torsion angle, the program calculates the sum of the $^{13}C$ anisotropic chemical shifts ($\omega_1$ dimension), the individual $^{13}C$ anisotropic chemical shifts, and the $^{13}C-^{13}C$ dipolar coupling ($\omega_2$ dimension). The double-quantum generation, dipolar/chemical-shift frequencies, and intensities were calculated according to the exact formulas.[26] Realistic line broadening to simulate the effects of paramagnetic impurities and susceptibility effects was generated by convolution with suitable Gaussian curves parallel and perpendicular to the line of slope 2. In the simulations, the principal values of the chemical shift tensor used were $\sigma_{11} = 93$ ppm, $\sigma_{22} = 84$ ppm, and $\sigma_{33} = 36$ ppm, the polar coordinates of the C−C bond in the chemical-shift principal-axis system (PAS) were $\alpha = -90°$, $\beta = 120°$, and $\gamma =$ torsion angle, and the effective distance between two adjacent carbons was set equal to 1.56 Å. Examples of simulated spectra obtained for torsion angles of 70 and 180° are shown in Figure 3.

**NMR Background.** In the following, we briefly review the principles of the double-quantum experiment.[20] We consider a pair of directly bonded $^{13}C$ nuclei with chemical shifts $\omega_a$ and $\omega_b$, and with a dipolar coupling Hamiltonian of $\hbar\omega_D(3S_zL_z - \vec{S}\cdot\vec{L})$. In the two-dimensional spectrum obtained, the orientation-dependent individual frequencies $\omega_a$ and $\omega_b$ in the second dimension are correlated with the torsion-angle dependent sum of frequencies ($\omega_a + \omega_b$) in the first (DQ) dimension. The resulting two-dimensional spectral pattern depends on the relative orientation and thus on the torsion angle between the $^{13}C$-containing segments.[20]

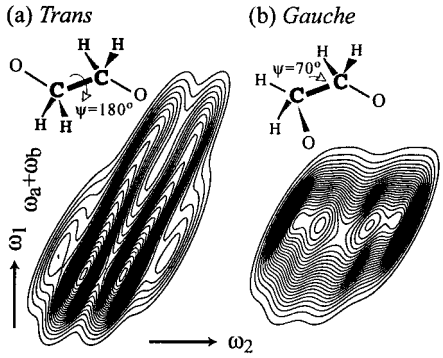


**Figure 3.** Examples of simulated two-dimensional double-quantum spectra for torsion angles equal to (a) 180° (trans) and (b) 70° (gauche).

From the initial transverse magnetization $S_y + L_y$, double-quantum (DQ) coherence $2S_xL_y + 2S_yL_x$ is generated by the dipolar coupling and radio frequency pulses of suitable phase:

$$\text{DQ excitation: } S_y + L_y \xrightarrow{H\tau\ 180^\circ\ H\tau} -(2S_xL_z + 2S_zL_x)g(2\tau) \xrightarrow{90^\circ_x} -(2S_xL_y + 2S_yL_x)g(2\tau) \quad (1a)$$

The DQ excitation factor $g(2\tau)$ is given below. The DQ coherence then evolves under the sum of frequencies $\omega_a + \omega_b$ during $t_1$:[27]

$$\text{DQ evolution: } \xrightarrow{Ht_1} -(2S_xL_y + 2S_yL_x)g(2\tau)\cos[(\omega_a + \omega_b)t_1] \quad (1b)$$

Modulated by $\cos[(\omega_a + \omega_b)t_1]$, the DQ coherence is reconverted into observable magnetization $S_y + L_y$:

$$\text{DQ reconv.: } \xrightarrow{90^\circ_{-x}} -(2S_xL_z + 2S_zL_x)g(2\tau)\cos[(\omega_a + \omega_b)t_1] \xrightarrow{H\tau\ 180^\circ\ H\tau} -(S_y + L_y)g^2(2\tau)\cos[(\omega_a + \omega_b)t_1] \quad (1c)$$

which is observed in the detection period $t_2$. The signal acquired during $t_2$, under continuous-wave proton decoupling, reflects the individual chemical shifts $\omega_a$ and $\omega_b$, and the $^{13}C-^{13}C$ dipole−dipole interaction. The dead-time problem is avoided by a solid echo with Hahn-echo sandwich before detection.[28] The two-dimensional time signal is thus

$$S(t_1,t_2) = g^2(2\tau)\cos[(\omega_a + \omega_b)t_1]f(t_2) \quad (2)$$

In an experiment with complete dipolar decoupling during detection,[28] $f(t_2) = \exp(i\omega_a t_2) + \exp(i\omega_b t_2)$, so that, in the 2D spectrum, signals of intensity $g^2(2\tau)$ are observed at ($\omega_a+\omega_b$, $\omega_a$) and ($\omega_a+\omega_b$, $\omega_b$).

The double-quantum excitation factor $g(2\tau)$, which is a function of $\Delta = \omega_a - \omega_b$ and $R = (\Delta^2 + \omega_D^2)^{1/2}$, is given in ref 26 in general terms. For our purposes, we find

$$g(2\tau) = \left(\left(\frac{\Delta}{R}\right)^2 + \left(\frac{\omega_D}{R}\right)^2 \cos R\tau\right)\sin\omega_D 2\tau + \frac{\omega_D}{R}\sin R\tau\cos\omega_D 2\tau \quad (3)$$

Note that, in Nakai and MacDowell's notation,[26] $A = B = \omega_D$ for the dipolar coupling and that we choose the full elapsed time $2\tau$, not just half of it, as the argument of the $g$ function.

In the very-strong-coupling limit, defined by $\Delta \ll \omega_D$, $R \approx \omega_D$ and both terms of eq 3 combined yield $g(2\tau) = \sin(1.5*\omega_D 2\tau)$.[29] In the weak-coupling limit, defined by $\Delta \gg$

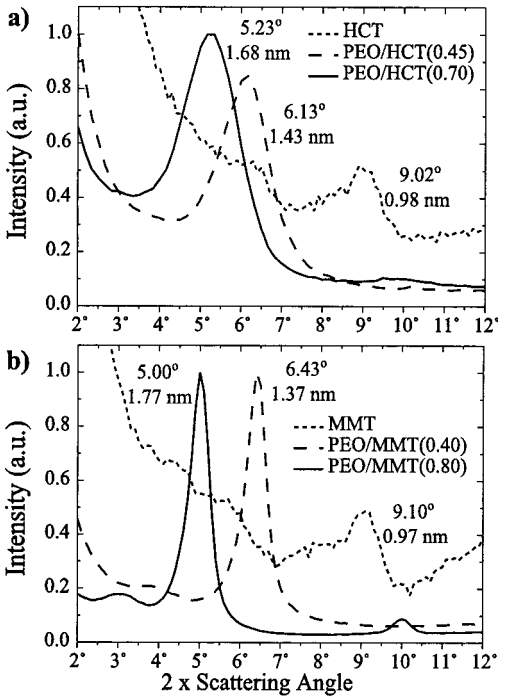


**Figure 4.** X-ray diffractograms of (a) HCT, PEO/HCT(0.45), and PEO/HCT(0.70) as studied by NMR and, for reference, (b) MMT, PEO/MMT(0.40), and PEO/MMT(0.80). These X-ray patterns show an increase in the separation of the original inorganic galleries by ca. 0.40 or 0.80 nm, indicating that the guest and the host have formed a nanocomposite.

**Table 2. Elemental Analyses for C, H, and Li in PEO/$MoS_2$(0.82)**

| *R* | Li wt % | C wt % | H Wt % | H/C | composition |
|---|---|---|---|---|---|
| 0.45 | 0.30 | 14.18 | 2.29 | 1.92 | $Li_{0.09}(PEO)_{1.28}MoS_2$ |

$\omega_D$, we have $R \approx \Delta \gg \omega_D$ so that the first term $g(2\tau) = \sin(\omega_D 2\tau)$ dominates. For $\Delta \approx \omega_D$, in the intermediate-coupling range, all terms in eq 3 are relevant.

**Sample Characterization.** Elemental analysis for C, H, and Li in the PEO/$MoS_2$(0.82) is given in Table 2. The ratios of these atoms are similar to those presented in a previous study.[2]

WAXD data of the nanocomposites show an increase in the separation of the original inorganic galleries by ca. 0.4 or 0.8 nm, indicating that the PEO and the hosts formed nanocomposites;[1] see parts a and b of Figure 4 and Figure 5a. The long period of the inorganic layers, *c*, is obtained from the (001) peak. Additional information about structure and intra- and interlayer atomic distances for pure and intercalated smectite clays and transition metal dichalcogenides were obtained from refs 30−33. Table 1 summarizes the long period of the inorganic layers, *c*, obtained from the X-ray experiments for each sample studied, as well as the estimated free interlayer gap width before and after intercalation, $gap_0$ and $gap_1$, respectively.

WAXD also confirms the suppression of the crystalline phase of PEO. In Figure 5b, it is seen that the peaks characteristic of crystalline PEO are absent in the PEO/$MoS_2$(0.82) data.

Figure 6 shows the DSC curves recorded in the range of −90 to +100 °C for neat PEO and intercalated nanocomposites. Figure 6a shows the characteristic behavior of neat PEO, where the large endotherm at 67 °C corresponds to the melting of the crystalline regions. The absence of a melting transition for all nanocomposites, see parts b−d of Figure 6, confirms that the confinement of polymer chains between the inorganic layers prevents crystallization[1−5,7−10] and indicates that all of the polymer is intercalated.

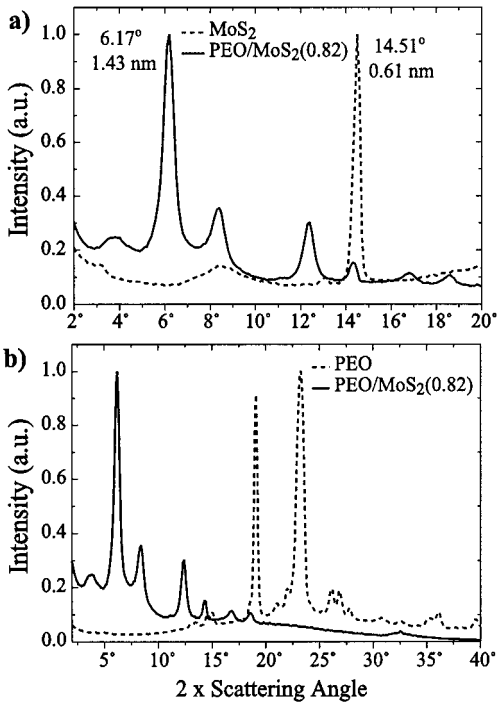


**Figure 5.** X-ray diffractograms of (a) $MoS_2$ and PEO/$MoS_2$-(0.82) and, for comparison, (b) PEO/$MoS_2$(0.82) and neat PEO. The X-ray patterns in part a show an increase in the separation of the original inorganic gallery by ca. 0.80 nm, indicating that the guest and the host formed a nanocomposite. In part b, the suppression of the PEO crystalline phase is observed for PEO/$MoS_2$(0.82).

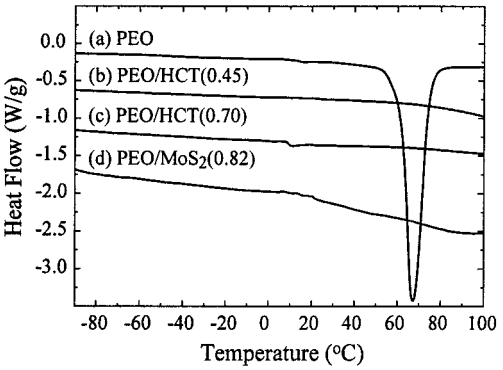


**Figure 6.** Differential scanning calorimetry traces for (a) neat PEO, (b) PEO/HCT(0.45), (c) PEO/HCT(0.70), and (d) PEO/$MoS_2$(0.82). Samples were heated at rate of 10 °C/min.

## Results and Discussion

**Double-Quantum NMR Spectra.** Figures 7 and 8 show the double-quantum 2D NMR spectra of the $^{13}C-^{13}C$ labeled PEO for the samples PEO/$MoS_2$(0.82), PEO/HCT(0.45), and PEO/HCT(0.70), with the corresponding simulations. The spectra show predominantly the pattern of the gauche conformation; see Figure 3b. Nevertheless, the extended features of the trans spectrum (see Figure 3a) are also observed faintly at the upper region of the spectra.

The 2D double-quantum spectra for both clay nanocomposites are similar. The trans:gauche ratios are 8:92(±5), with average gauche and trans angles equal to 70 ± 15 and ∼180°, respectively. Because of the low trans content, a reliable estimate of the uncertainty of the trans torsion angle is difficult. For the PEO/$MoS_2$-(0.82) compound, the trans:gauche ratio was found to

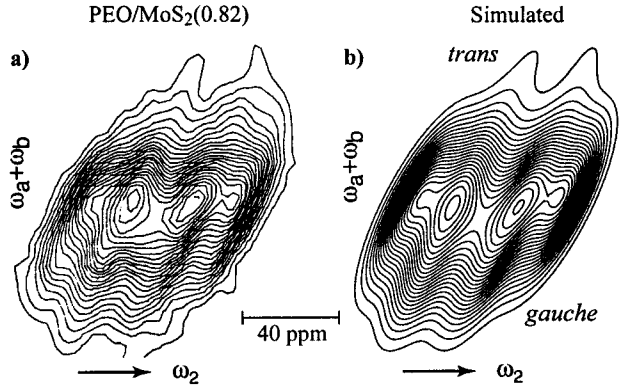


**Figure 7.** Experimental 2D double-quantum NMR spectrum of (a) PEO/$MoS_2$(0.82) and (b) the corresponding simulation using a trans content of 12%. The trans and gauche angles were distributed within ±10° around 180 and 70°, respectively. Contour lines were plotted between 5 and 98% of the maximum.

be 12:88(±5), with average gauche and trans angles equal to 70 ± 15 and ∼180°. In the simulations, distributions with widths of 10° around the average trans and gauche torsion angles of 180 and 70° were used.

The experimental spectra show significant broadening, in particular along the line of slope 2, which shows that the broadening for both coupled spins is correlated. It is probably due to paramagnetic impurities or to susceptibility effects. The chemical shift dispersion due to conformational and packing effects is a less likely reason. These effects would not cause such large line widths and the broadenings for the two bonded sites would be expected to be mostly uncorrelated. To avoid distortion of the line shape by segmental dynamics, the samples were cooled to 220−225 K. Cooling to lower temperatures did not lead to significant line-shape changes.

The high gauche content clearly excludes a planar all-trans conformation. The low trans:gauche ratio also indicates that a regular planar structure with 33% trans as found in the complex of PEO with *p*-nitrophenol[34] is not predominant. The conformational statistics and estimate of the width of the gauche conformation peak in the torsion angle distribution will be useful as benchmarks for simulations of intercalated PEO chains.

**Comparison with Previous Spectroscopic Results.** Aranda and Ruiz-Hitzky[5] had shown that the $^{13}C$ CP/MAS NMR spectrum of PEO/$Na^+$−hectorite with gallery expansion of 0.8 nm had only one peak at 69.6 ppm, which was assigned to the gauche conformation of methylene groups, suggesting that the helical conformation is maintained after intercalation. However, given the range of the chemical shift resonances in neat PEO, the relation between the chemical shift and the C−C torsion is tentative at best.[35] Actually, in PEO the torsion angle of the C−C bond cannot lead to a $\gamma$-gauche shielding; only C−O torsion angles can lead to this effect. In addition, the MAS lines of PEO in hectorite and $MoS_2$ nanocomposites are 15 ppm broad, which makes it impossible to observe any fine structure indicative of specific conformations or packing.

Aranda and Ruiz-Hitzky[5] also had analyzed the interaction between ether oxygens and interlayer cations using $^{23}Na$ NMR spectroscopy for PEO/$Na^+$−hectorite with gallery expansion of 0.8 nm. The comparison of the $^{23}Na$ spectra of dry, hydrated, and PEO intercalated hectorites had shown an 11 ppm downfield shift of the $^{23}Na$ peak after intercalation of hectorite with PEO, suggesting that the $Na^+$ ions interact strongly with the ether oxygens. A dibenzo-24-crown-8/hectorite intercalate had a similar $^{23}Na$ spectrum ($\delta = -10.3$ ppm) to those of PEO/hectorite intercalates. A high OC−CO gauche content as found in this study is consistent with PEO segments in crown-ether-like conformations. On the other hand, $^7Li$ NMR line widths observed by Yang and Zax[36] suggest that $Li^+$ ions are restricted to the silicate surface.

$^7Li$ and $^2H$ solid-state NMR had been used by Wong et al.[21,37,38] to probe the dynamics of the $Li^+$ ion and the polymer in deuterated PEO/$Li^+$−fluorohectorite intercalates. The temperature dependences of the quadrupolar NMR powder patterns of both nuclei indicate that PEO, even at 220 K, possesses some small-amplitude dynamics. At higher temperatures, even above the bulk melting point of PEO (65 °C), the spectra exhibit residual powder patterns in addition to an intense single line, indicating restricted polymer motion between silicate layers. In addition, they indicate that there is a competition of the oxygen ethers of PEO with the surface oxygens of the silicate layers for interaction with the $Li^+$ cation. IR studies also indicate interaction between polymer and interlayer cations.[5]

Papke et al.[39] and Yokoyama et al.[40] had used vibrational spectroscopy to study PEO in metal salt complexes to elucidate chain conformations. The analy-

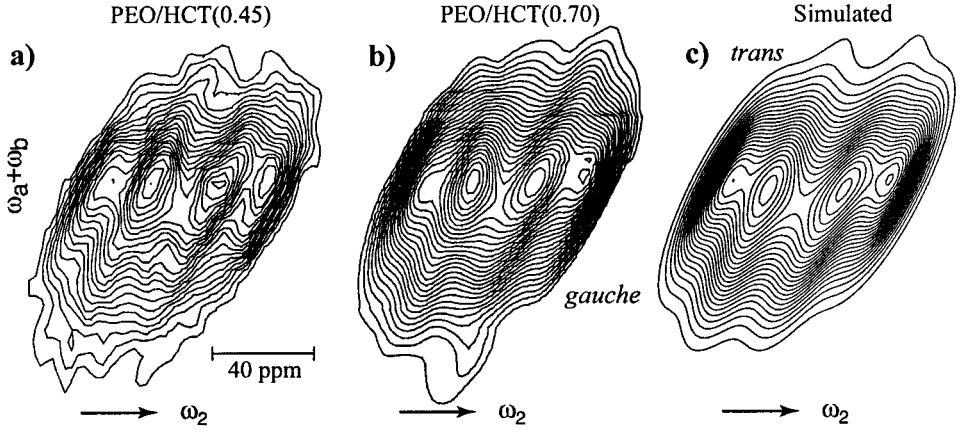


**Figure 8.** 2D double-quantum NMR spectra of (a) PEO/HCT(0.45) and (b) PEO/HCT(0.70) with (c) the corresponding simulation using a trans content of 8%. The trans and gauche angles were distributed within ±10° around 180° and 70°, respectively. The uncertainty in the average gauche torsion angle is ±15°.

sis of $CH_2$ deformation bands of $O-CH_2-CH_2-O$ groups reveals trans or gauche conformations, and consequently it was possible to ascribe a helical structure for alkaline metal salt complexes ($TTGTT\bar{G}$)[39] or, alternatively, a nearly planar conformation in certain PEO/$HgCl_2$ salt complexes ($TGGT\bar{G}\bar{G}$).[40] Aranda and Ruiz-Hitzky[5] had used vibrational-spectroscopy studies to elucidate PEO chain conformations in intercalated clays. In PEO intercalates with gallery expansion of 0.8 nm, the spectra suggest a gauche conformation, which was taken to show that the matrix structure of PEO is preserved after intercalation. While the NMR results agree with a dominance of gauche, the observed trans content shows that very long helical sections are not possible.

**Possible Chain Conformations.** The rotational isomeric state (RIS) description of amorphous PEO[41,42] can be used to understand the chain conformations in the intercalated materials. The RIS model for amorphous PEO suggests that the energy of trans CO−CC bonds is approximately 900 cal/mol greater than that of the gauche conformations. Approximately 25% of the CO−CC bonds are gauche in amorphous PEO. The energy of gauche OC−CO bonds is 400 cal/mol greater than that of the trans conformation and approximately 20% of these bonds are trans in the amorphous state. The 10 ± 5% trans population of the OC−CO bonds observed for intercalated PEO is less than the predicted value from the RIS description of amorphous PEO. If this difference is correct and the values of the RIS description are accurate, it may be due to either interaction with interlayer ions and the interface, or steric requirements. Regarding the latter, it is interesting to note that RIS simulations of PEO chains confined to channels of 0.8 nm diameter[43] predict a trans fraction of 50%, even though the crystalline $7_2$ helix, with 100% gauche OC−CO bonds, would fit the channels.

To accommodate the large fraction of OC−CO bonds in the gauche conformation yet allowing the chain to remain mostly planar, some sequences of conformations will be restricted. The gauche OC−CO bonds cannot be randomly gauche$^+$ and gauche$^-$, but rather will be strongly correlated with nearby gauche bonds. If all of the gauche OC−CO bonds in a long chain section have the same sign, i.e., either all are gauche$^+$ or all gauche$^-$, the chain twists into a helix. The helix would fit into the intercalation gap, but a trans conformation at its end would almost invariably be in steric conflict with the inorganic layers.

If the signs of the OC−CO gauche torsion angles alternate, the chain loops into a structure similar to small crown ethers with the ether oxygens directed inward. This would be consistent with strong polymer−$Na^+$ interactions deduced from $^{23}Na$ NMR.[5] However, after approximately five monomer units with alternating $TTG^+$ and $TTG^-$ conformations, either a OC−CO bond would be forced into a trans conformation or a CO−CC bond would be forced into a gauche conformation due to steric interactions with other portions of the chain. The observed trans fraction of OC−CO bonds for the studied systems is only 10%, lower than the ∼25% that would be required due to these steric interactions. We therefore expect that a significant percentage of the CO−CC bonds are in the gauche conformation. This significant percentage would not conflict with the values predicted by the RIS description.

## Conclusions

The conformations of the OC−CO bonds of PEO intercalated in hectorite clay and in $MoS_2$ have been studied by double-quantum solid-state NMR. The polymer chains are confined into intercalation gaps of well-defined thicknesses of only ∼0.8, ∼0.85, and ∼1.0 nm, as determined by WAXD. The OC−CO bonds are found to be 90 ± 5% gauche, which provides valuable constraints on the possible chain conformation in the intercalation gaps.

**Acknowledgment.** Financial support by the Arnold and Mabel Beckman Foundation is gratefully acknowledged. Partial support was also provided by NSF/MRSEC. T.J.B. thanks the Fundação de Amparo à Pesquisa do Estado de São Paulo (FAPESP)—Brazil for a fellowship. A. J. Waddon helped with X-ray, J. Morin helped with DSC, and G. M. Dabkowski provided the elemental analyses.

## References and Notes

(1) Wu, J.; Lerner, M. M. *Chem. Mater.* **1993**, *5*, 835.
(2) Lemmon, J. P.; Lerner, M. M. *Chem. Mater.* **1994**, *6*, 207.
(3) Lemmon, J. P.; Lerner, M. M. *Solid State Commun.* **1995**, *94*, 533.
(4) Oriakhi, C. O.; Nafshun, R. L.; Lerner, M. M. *Mater. Res. Bull.* **1996**, *31*, 1513.
(5) Aranda, P.; Ruiz-Hitzky, E. *Chem. Mater.* **1992**, *4*, 1395.
(6) Ruiz-Hitzky, E.; Jimemez, R.; Casal, B.; Manriquez, V.; Ana, A. S.; Gonzalez, G. *Adv. Mater.* **1993**, *5*, 738.
(7) Aranda, P.; Ruiz-Hitzky, E. *Acta Polym.* **1994**, *45*, 59.
(8) Vaia, R. A.; Vasudevan, S.; Krawiec, W.; Scanlon, L. G.; Gianellis, E. P. *Adv. Mater.* **1995**, *7*, 154.
(9) Giannelis, E. *Adv. Mater.* **1996**, *8*, 29.
(10) Vaia, R. A.; Sauer, B. B.; Tse, O. K.; Gianellis, E. P. *J. Polym. Sci., Part B: Polym. Phys.* **1997**, *35*, 59.
(11) Vaia, R. A.; Ishii, H.; Giannelis, E. P. *Chem. Mater.* **1993**, *5*, 1694.
(12) Vaia, R. A.; Jandt, K. D.; Kramer, E. J.; Giannelis, E. P. *Macromolecules* **1995**, *28*, 8080.
(13) Krishnamoorti, R.; Vaia, R. A.; Giannelis, E. P. *Chem. Mater.* **1996**, *8*, 1728.
(14) Vaia, R. A.; Giannelis, E. P. *Macromolecules* **1997**, *30*, 7990.
(15) Vaia, R. A.; Giannelis, E. P. *Macromolecules* **1997**, *30*, 8000.
(16) Ogawa, M.; Kuroda, K. *Chem. Rev.* **1995**, *95*, 399.
(17) Tadokoro, H.; Chatani, Y.; Kobayashi, M.; Yoshihara, T.; Murahashi, S.; Yamada, K. *Rep. Prog. Polym. Phys. Jpn.* **1963**, *6*, 303.
(18) Tadokoro, H.; Chatani, Y.; Yoshihara, T.; Tahara, S.; Murahashi, S. *Makromol. Chem.* **1964**, *74*, 109.
(19) Takahashi, Y.; Tadokoro, H. *Macromolecules* **1973**, *6*, 672.
(20) Schmidt-Rohr, K. *Macromolecules* **1996**, *29*, 3975.
(21) Wong, S.; Zax, D. B. *Electrochim. Acta* **1997**, *2*, 3513.
(22) Divigalpitiya, W. M. R.; Frindt, R. F.; Morrison, S. R. *Science* **1989**, *246*, 369.
(23) Dines, M. B. *Mater. Res. Bull.* **1975**, *10*, 287.
(24) Schmidt-Rohr, K.; Spiess, H. W. *Multidimensional solid-state NMR and polymers*, 1st ed.; Academic Press: San Diego, CA, 1994.
(25) Schmidt-Rohr, K. *J. Am. Chem. Soc.* **1996**, *118*, 7601.
(26) Nakai, T.; MacDowell, C. A. *Mol. Phys.* **1993**, *79*, 965.
(27) The bilinear terms in eq 2 of our previous work[20] lack prefactors of −2, which are correctly included in eq 1 in this paper.
(28) Schmidt-Rohr, K. *J. Magn. Reson.* **1998**, *131*, 209−217.
(29) In ref 20 the prefactor $q(-2)$ in the expression for $g(2\tau)$ as given below eq 2 of that reference is incorrect and has to be dropped. The simulated spectra, whose line shape would be unaffected by an overall prefactor anyways, were calculated using the correct full expression of ref 26.
(30) Dickinson, R. G.; Pauling, L. *J. Am. Chem. Soc.* **1923**, *45*, 1466.
(31) Grim, R. E. *Clay Mineralogy*, 1st ed.; McGraw-Hill Book Company: New York, 1953.
(32) Whittingham, M. S. *Prog. Solid State Chem.* **1978**, *12*, 41.
(33) Pinnavaia, T. J. *Science* **1983**, *220*, 365.
(34) Damman, P.; Point, J. J. *Macromolecules* **1993**, *26*, 1722.

(35) Schilling, F. C.; Tonelli, A. E.; Cholli, A. *J. Polym. Sci., Part B: Polym. Phys.* **1992**, *30*, 91.
(36) Yang, D.-K.; Zax, D. B. *J. Chem. Phys.* **1999**, *110*, 5325.
(37) Wong, S.; Vasudevan, S.; Vaia, R. A.; Gianellis, E. P.; Zax, B. *J. Am. Chem. Soc.* **1995**, *117*, 7568.
(38) Wong, S.; Vaia, R. A.; Gianellis, E. P.; Zax, D. B. *Solid Sate Ionics* **1996**, *86*−*88*, 547.
(39) Papke, B. L.; Ratner, M. A.; Shriver, D. F. *J. Phys. Chem. Solids* **1981**, *42*, 493.
(40) Yokoyama, M.; Ishihara, H.; Iwamoto, R.; Tadokoro, H. *Macromolecules* **1969**, *2*, 184.
(41) Mark, J. E.; Flory, P. J. *J. Am. Chem. Soc.* **1965**, *87*, 1415−1422.
(42) Mark, J. E.; Flory, P. J. *J. Am. Chem. Soc.* **1966**, *88*, 3702−3707.
(43) Tonelli, A. E. *Macromolecules* **1990**, *23*, 3134−3137.

MA9907800